

change/delete REPORT-#
February 25, 2024

Rare B meson decays at the Tevatron

WALTER HOPKINS FOR THE CDF AND D0 COLLABORATIONS

Cornell University, Ithaca, NY 14853

Abstract

Rare B meson decays are an excellent probe for beyond the Standard Model physics. Two very sensitive processes are the $B_{s,d}^0 \rightarrow \mu^+ \mu^-$ and $b \rightarrow s \mu^+ \mu^-$ decays. We report recent results at a center of mass energy of $\sqrt{s} = 1.96$ TeV from the CDF II and D0 collaborations using between 3.7 fb $^{-1}$ and 6.9 fb $^{-1}$ taken during Run II of the Fermilab Tevatron Collider.

PRESENTED AT

The Ninth International Conference on
Flavor Physics and CP Violation
(FPCP 2011)
Maale Hachamisha, Israel, May 23–27, 2011

1 $b \rightarrow s\mu^+\mu^-$ decays

$b \rightarrow s\mu^+\mu^-$ decays are flavor changing neutral current (FCNC) processes that can only occur through higher order box or penguin amplitudes in the Standard Model. New physics can be probed by measuring various combinations of their decay rates. One of the most sensitive observables is the forward-backward asymmetry of the muons (A_{FB}) as a function of the squared di-muon mass.

Three decays of interest are $B^+ \rightarrow \mu^+\mu^-K^+$, $B_d^0 \rightarrow \mu^+\mu^-K^*(892)^0$, and $B_s^0 \rightarrow \mu^+\mu^-\phi$. The first two decays were observed at BaBar, Belle, and CDF. Belle found a 2.7σ deviation for A_{FB} for $B_d^0 \rightarrow l^+l^-K^*$ [1]. We describe here the CDF analysis that uses 4.4 fb^{-1} of data [2].

1.1 Analysis Method

1.1.1 Branching Ratio Measurement

Branching ratios for $B_d^0 \rightarrow \mu^+\mu^-K^*(892)^0$, $B^+ \rightarrow \mu^+\mu^-K^+$, and $B_s^0 \rightarrow \mu^+\mu^-\phi$ are measured relative to normalization modes, where the two muons originate from a J/ψ decay. For the event reconstruction CDF requires two muons with a transverse momentum (p_T) greater than either 1.5 GeV/c or 2.0 GeV/c depending on the muon trigger. The three modes are then reconstructed where the $K^*(892)^0$ is reconstructed from $K^*(892)^0 \rightarrow K^+\pi^-$ and the ϕ is reconstructed from $\phi \rightarrow K^+K^-$. To avoid contamination from resonant modes such as the J/ψ and ψ' , candidates with di-muon masses near these resonances are rejected.

The events then have to meet loose preselection requirements before an artificial neural network (NN), which combines multiple discriminating variables into one variable, is applied. Signal is modeled with p_T -reweighted Pythia signal Monte Carlo simulations (MC). The reweighting is done by comparing the MC p_T distribution with that of the normalization modes. The background is modeled by sampling the B meson mass sideband regions. For the $B_d^0 \rightarrow \mu^+\mu^-K^*(892)^0$ and $B^+ \rightarrow \mu^+\mu^-K^+$ modes there are significant physics backgrounds in the lower sideband region and thus only the higher sideband region between 5σ and 15σ ($\sigma=20\text{MeV}/c^2$) above the known B meson masses is used. For $B_s^0 \rightarrow \mu^+\mu^-\phi$ both lower and upper sidebands are used.

The final signal yield is obtained by an unbinned maximum likelihood fit to the B meson mass distribution. The probability distribution function (PDF) of the signal is parametrized with two Gaussian with different means while the background PDF is described by a first or second order polynomial. Peaking background contributions are subtracted from the fit results for the signal yields. The only significant peaking contribution is cross-talk among $B_d^0 \rightarrow \mu^+\mu^-K^*(892)^0$ and $B_s^0 \rightarrow \mu^+\mu^-\phi$ which has a $\sim 1\%$ contribution to the total observed signal MC yields. The final branching ratios are calculated as follows:

$$\mathcal{B}(B \rightarrow h\mu^+\mu^-) = \frac{N_{h\mu^+\mu^-}^{\text{NN}}}{N_{J/\psi h}^{\text{loose}}} \cdot \frac{\epsilon_{J/\psi h}^{\text{loose}}}{\epsilon_{h\mu^+\mu^-}^{\text{loose}}} \frac{1}{\epsilon_{h\mu^+\mu^-}^{\text{NN}}} \cdot \mathcal{B}(J/\psi h) \cdot \mathcal{B}(J/\psi \rightarrow \mu^+\mu^-), \quad (1)$$

where B signifies the B_d^0 , B^+ , or B_s^0 and h represents $K^*(892)^0$, K^+ , or ϕ , $N_{h\mu^+\mu^-}^{\text{NN}}$ and $N_{J/\psi h}^{\text{loose}}$ are the yields after the optimal NN, $\frac{\epsilon_{J/\psi h}^{\text{loose}}}{\epsilon_{h\mu^+\mu^-}^{\text{loose}}}$ is the relative efficiency of the loose selection cuts, and $\epsilon_{h\mu^+\mu^-}^{\text{NN}}$ is the NN cut efficiency on the loosely-selected events. The NN is not applied to the normalization mode because the signal/purity and size is sufficient with the loose selection cuts. The NN cut efficiency are obtained from signal MC.

The three leading systematics are the systematics on the efficiency, $\mathcal{B}(J/\psi h)$, and background PDF. The main sources within the efficiency systematic errors are the MC reweighing and the NN cut. The total systematics for the $B_d^0 \rightarrow \mu^+\mu^-K^*(892)^0$, $B^+ \rightarrow \mu^+\mu^-K^+$, and $B_s^0 \rightarrow \mu^+\mu^-\phi$ are 9%, 7%, and 32%, respectively.

1.1.2 Forward-Backward Asymmetry Measurement

For the $B_d^0 \rightarrow \mu^+\mu^-K^*(892)^0$ decay the forward-backward asymmetry (A_{FB}) as well as the K^* longitudinal polarization (F_L) are measured. These are extracted from $\cos\theta_\mu$, the cosine of the helicity angle between the μ^+ (μ^-) momentum vector and the opposite of B (\bar{B}) meson momentum vector in the di-muon rest frame, and $\cos\theta_K$, the cosine of the angle between kaon momentum and the opposite of the B meson momentum vector in the $K^*(892)^0$ rest frame. B decay amplitudes are calculated using operator product expansion and Wilson coefficients. There are many non-SM predictions for A_{FB} from models with different Wilson coefficients [3].

A_{FB} and F_L are extracted using a unbinned maximum likelihood fit containing B mass shape signal and background PDF's as well as signal and background angular shape PDF's. The mass shape PDF's are divided into several di-muon mass bins and are described as 25 bin histograms. The combinatorial background PDF is taken from the B meson higher sideband. The angular acceptances are also described as 25 bin histograms and are derived from phase space signal MC.

As a control A_{FB} and F_L are fitted to $B_d^0 \rightarrow J/\psi K^*(892)^0$ and A_{FB} only to $B^+ \rightarrow J/\psi K^+$. This cross check yielded measurements that were consistent with other measurements.

The systematic uncertainties for the F_L measurement in $B_d^0 \rightarrow \mu^+\mu^-K^*(892)^0$ are dominated by a fit bias ranging between 2% and 7% for the different di-muon mass bins. This bias affects the estimates of A_{FB} or F_L when the true value of these quantities are close to physical boundaries. The lowest di-muon mass bin also has a significant contribution from the angular efficiency systematic ($\sim 5\%$) attained

from changing the binning of the angular acceptance histograms. The total of all the systematics ranges between 2% and 8% for the different di-muon mass bins.

For the A_{FB} measurement in $B_d^0 \rightarrow \mu^+ \mu^- K^*(892)^0$ the dominant systematic uncertainties are the angular efficiency, fit bias, and the statistical uncertainty from the F_L fit. The F_L fit systematic comes from varying F_L by $\pm 1\sigma$ where σ is the statistical error from the F_L fit. The total systematic errors range is 1%-10%.

The most significant systematic uncertainties in the A_{FB} measurement for $B^+ \rightarrow \mu^+ \mu^- K^+$ is given by the angular efficiency and angular background. Angular background is estimated from the B higher mass sideband. The systematic is estimated by changing the sideband region. The total systematic uncertainty ranges between 3% and 8% for the different di-muon mass bins.

1.2 Results

The resulting yield for the three decays are shown in Figure 1. All measured branching ratios agree with previous measured values as well as theoretical predictions. CDF reports the first observation of $B_s^0 \rightarrow \mu^+ \mu^- \phi$ with a significance of $\sim 6\sigma$ and a measured branching ratio of $\mathcal{B}(B_s^0 \rightarrow \mu^+ \mu^- \phi) = (1.44 \pm 0.33[\text{stat}] \pm 0.46[\text{syst}]) \times 10^{-6}$.

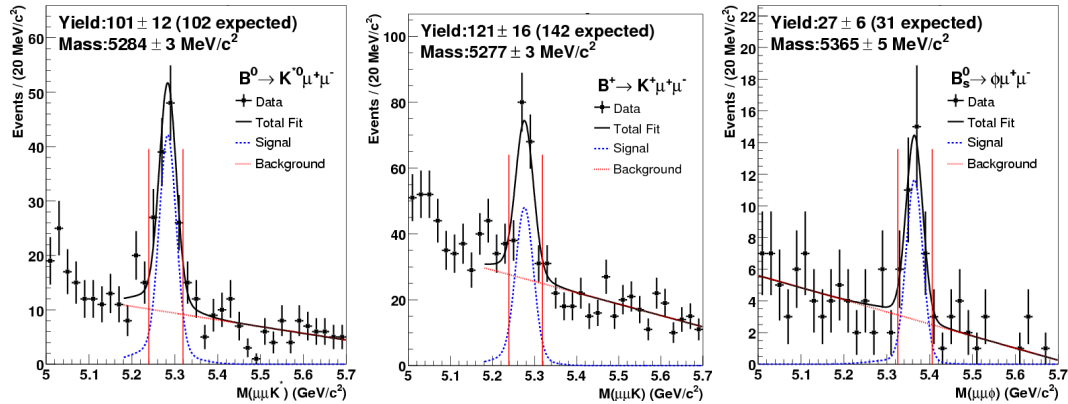


Figure 1: Yields for $B_d^0 \rightarrow \mu^+ \mu^- K^*(892)^0$, $B^+ \rightarrow \mu^+ \mu^- K^+$, and $B_s^0 \rightarrow \mu^+ \mu^- \phi$ from left to right. In all histograms the red vertical lines indicate the signal regions.

The results of the polarization and forward-backward asymmetry measurement shown in Figure 2 (A_{FB} for $B^+ \rightarrow \mu^+ \mu^- K^+$ is shown as a cross check) may contribute to constrain several beyond SM physics models. They are compatible and competitive with the results from the B-factories [1], [4], [5].

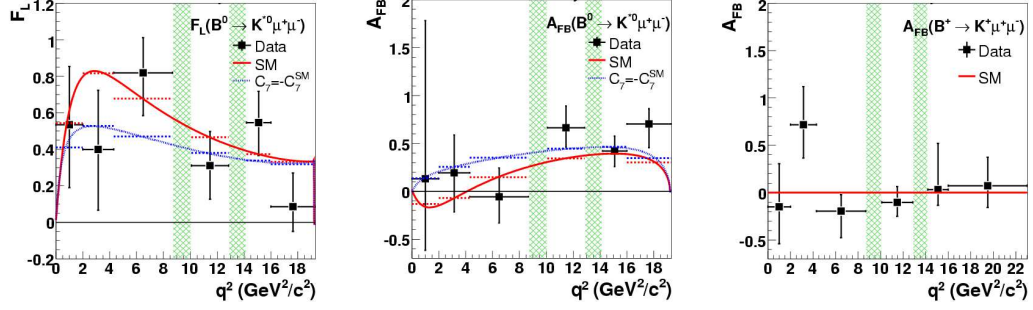


Figure 2: K^* Longitudinal Polarization, A_{FB} for $B_d^0 \rightarrow \mu^+ \mu^- K^*(892)^0$, and A_{FB} for $B^+ \rightarrow \mu^+ \mu^- K^+$ (from left to right). The green hatched areas are due to the charmonium veto (J/ψ , ψ').

2 $B_{s,d}^0 \rightarrow \mu^+ \mu^-$ decays

$B_{s,d}^0 \rightarrow \mu^+ \mu^-$ are FCNC decays that are highly suppressed by the SM. The SM predictions for these branching fractions are $\mathcal{B}(B_s^0 \rightarrow \mu^+ \mu^-) = (3.2 \pm 0.2) \times 10^{-9}$ and $\mathcal{B}(B_d^0 \rightarrow \mu^+ \mu^-) = (1.00 \pm 0.1) \times 10^{-10}$ [6]. These predictions are one order of magnitude smaller than the current experimental sensitivity. Previous bounds from the CDF collaboration, based on 3.7 fb^{-1} of integrated luminosity, are $\mathcal{B}(B_s^0 \rightarrow \mu^+ \mu^-) < 4.3 \times 10^{-8}$ and $\mathcal{B}(B_d^0 \rightarrow \mu^+ \mu^-) < 7.6 \times 10^{-9}$ at 95% C.L. [7]. D0 bounds were previously set at $\mathcal{B}(B_s^0 \rightarrow \mu^+ \mu^-) < 5.1 \times 10^{-8}$ at 95% C.L. using 6.1 fb^{-1} of data [8]. LHCb bounds of $\mathcal{B}(B_s^0 \rightarrow \mu^+ \mu^-) < 5.6 \times 10^{-8}$ and $\mathcal{B}(B_d^0 \rightarrow \mu^+ \mu^-) < 15 \times 10^{-9}$ at 95% C.L were recently set using 37 pb^{-1} of data

Enhancements to the rate of $B_s^0 \rightarrow \mu^+ \mu^-$ decays occur in a variety of different new-physics models. In supersymmetric (SUSY) models, new particles can increase $\mathcal{B}(B_s^0 \rightarrow \mu^+ \mu^-)$ by several orders of magnitude at large $\tan\beta$. In the minimal supersymmetric standard model (MSSM), the enhancement is proportional to $\tan^6\beta$. Global analysis including all existing experimental constraints suggest that the large $\tan\beta$ region is of interest [10, 11, 12]. For large $\tan\beta$, this search is one of the most sensitive probes of new physics available at the Tevatron experiments. In contrast, SUSY R-parity violating models [10] and non-minimal flavor violating models [13] can both enhance $B_s^0 \rightarrow \mu^+ \mu^-$ and $B_d^0 \rightarrow \mu^+ \mu^-$ separately even at low $\tan\beta$. In the absence of an observation, limits on $\mathcal{B}(B_s^0 \rightarrow \mu^+ \mu^-)$ are complementary to those provided by other experimental measurements, and together would constrain the allowed supersymmetric parameter space.

This document describes current status from D0 and CDF, as well as the planned updated analysis by CDF.

2.1 Analysis Method

Both CDF and D0 collect opposite sign muon candidate events using di-muon triggers.

$B^+ \rightarrow J/\psi K^+$ events are collected on the same triggers as a relative normalization mode to estimate $\mathcal{B}(B_s^0 \rightarrow \mu^+ \mu^-)$ as:

$$\mathcal{B}(B_s^0 \rightarrow \mu^+ \mu^-) = \frac{N_{B_s^0}}{\alpha_{B_s^0} \epsilon_{B_s^0}^{\text{total}}} \cdot \frac{\alpha_{B^+} \epsilon_{B^+}^{\text{total}}}{N_{B^+}} \cdot \frac{f_u}{f_s} \cdot \mathcal{B}(B^+ \rightarrow J/\psi K^+) \cdot \mathcal{B}(J/\psi \rightarrow \mu^+ \mu^-), \quad (2)$$

where $N_{B_s^0}$ is the number of candidate $B_s^0 \rightarrow \mu^+ \mu^-$ events, $\alpha_{B_s^0}$ is the geometric and kinematic acceptance of the di-muon trigger for $B_s^0 \rightarrow \mu^+ \mu^-$ decays, $\epsilon_{B_s^0}^{\text{total}}$ is the total efficiency (including trigger, reconstruction and analysis requirements) for $B_s^0 \rightarrow \mu^+ \mu^-$ events in the acceptance, with N_{B^+} , α_{B^+} , and $\epsilon_{B^+}^{\text{total}}$ similarly defined for $B^+ \rightarrow J/\psi K^+$ decays. The ratio f_u/f_s accounts for the different b -quark fragmentation probabilities and is $(0.402 \pm 0.013)/(0.112 \pm 0.013) = 3.589 \pm 0.374$, including the (anti-)correlation between the uncertainties [14]. The final two terms are the relevant branching ratios $\mathcal{B}(B^+ \rightarrow J/\psi K^+) \cdot \mathcal{B}(J/\psi \rightarrow \mu^+ \mu^-) = (1.01 \pm 0.03) \times 10^{-3} \cdot (5.93 \pm 0.06) \times 10^{-2} = (6.01 \pm 0.21) \times 10^{-5}$ [14].

The CDF analysis described is also sensitive to $B_d^0 \rightarrow \mu^+ \mu^-$ decays. The value of $\mathcal{B}(B_d^0 \rightarrow \mu^+ \mu^-)$ is estimated from Equation 2 substituting B_d^0 for B_s^0 , and changing f_u/f_s to $f_u/f_d = 1$. All other aspects are the same as the $B_s^0 \rightarrow \mu^+ \mu^-$ search except where noted below. The analysis is done by first estimating the acceptances

and efficiencies, then creating a multivariate discriminant for background rejection. This discriminant is optimized with Pythia signal MC and data mass sideband and validated with the $B^+ \rightarrow J/\psi K^+$ normalization. The background is then estimated, which has two sources: combinatorial background and peaking background ($B \rightarrow h^+ h^-$). Finally when the background is well understood the signal region is unblinded.

2.2 Signal and Background Properties

The signal candidates are fully reconstructed events with a secondary vertex due to the long lifetime ($\sim 450 \mu\text{m}$) of the B_s^0 meson. Signal events will have a primary-to-secondary vertex vector that is aligned with the B_s^0 candidate momentum vector (Figure 3). Another property of signal events that is unique is that they are very isolated (with few tracks near the muon tracks) due to the hard B fragmentation.

Background events tend to be partially reconstructed and be shorter lived than signal. They also have a softer p_T spectrum, higher activity of tracks, and misaligned primary-to-secondary vertex and momentum vectors. The combinatorial background consists of sequential semi-leptonic decay ($b \rightarrow c \mu^- X \rightarrow \mu^+ \mu^- X$) and double semi-leptonic decay ($bb \rightarrow \mu^- \mu^+ X$). The expected number of combinatorial back-

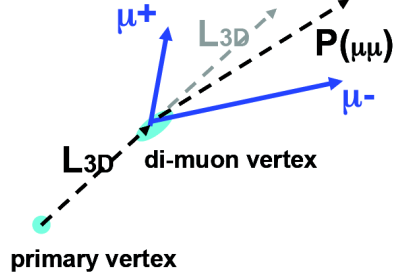


Figure 3: Sketch of the decay topology.

ground events in the signal window is estimated by extrapolating the number of events in the sideband regions to the signal window using a first order polynomial fit.

The peaking background from two-body hadronic B decays is also evaluated. These backgrounds are about a factor ten smaller than the combinatorial background and need to be estimated separately. The dominant sources of background are the decays of B_s^0 and B^0 to $h^+h'^-$ final states, where h or h' can be either π^\pm or K^\pm and are misreconstructed (fake muons).

2.3 CDF Analysis with 3.7 fb^{-1} of Data

2.3.1 Signal Discrimination

Six variables are used for the signal discrimination (Figure 4). Three of the variables are secondary vertex variables. These variables are combined in an artificial neural network which is optimized with signal MC and data mass sidebands (Figure 4, left). The NN output is then divided into three bins while the di-muon mass is split into 5 mass bins for limit calculation.

λ : the proper decay length;

$\Delta\alpha$: the 3D opening angle between the B_s^0 flight direction, $\vec{p}(B)$, and the direction of the decay vertex - estimated as the vector originating at the primary vertex and terminating at the muon-pair vertex;

Iso: the isolation of the candidate B_s^0 defined as $Iso = p_T^{B_s^0} / (p_T^{B_s^0} + \sum_i p_T^i (\Delta R < 1.0))$, where the sum is over all tracks within an $\eta - \phi$ cone of radius $R = 1.0$, centered on $\vec{p}(B)$;

λ/σ_λ : proper decay length significance (λ divided by the uncertainty on λ);

$\mathbf{p_T}(B_s^0)$: the transverse momentum of the B_s^0 candidate;

$\mathbf{p_T}(\mu)$: the transverse momentum of lower momentum daughter muon.

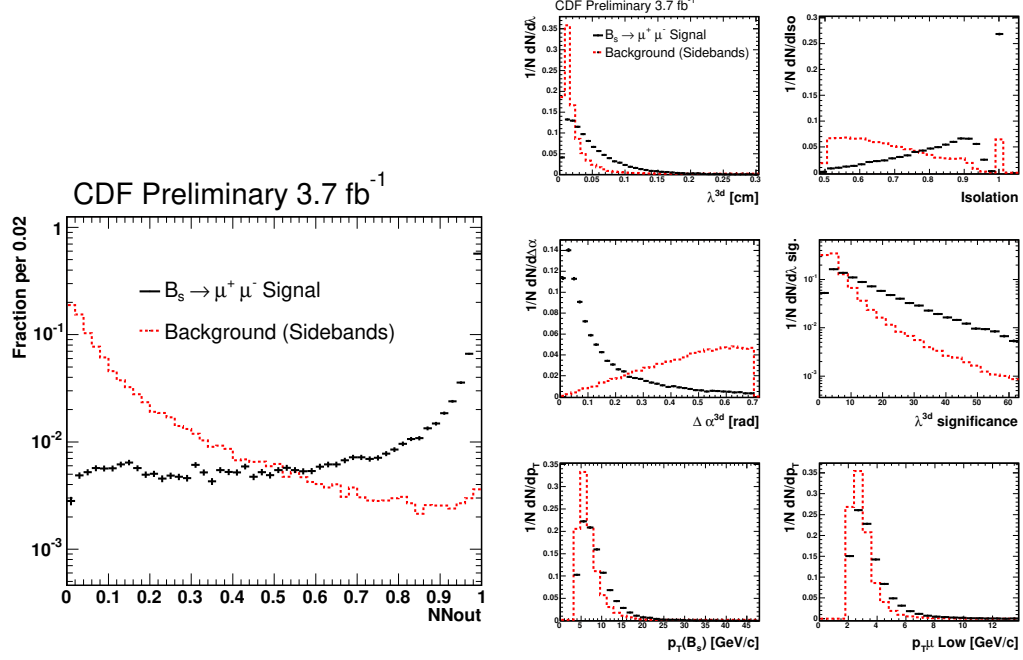


Figure 4: **Left**: Neural network output for signal MC and data mass sideband. **Right**: Distributions of neural network input variable for signal MC and data mass sideband.

2.3.2 Control Samples for Combinatorial Background Estimates

CDF cross checked the background estimate procedure on four independent background samples:

- OS-**: opposite-sign muon pairs, which pass the baseline and vertex cuts and have a negative lifetime;
- SS+**: same-sign muon pairs, which pass looser baseline and vertex cuts and have a positive lifetime;
- SS-**: same-sign muon pairs, which pass looser baseline and vertex cuts and have a negative lifetime;
- FM+-**: opposite-sign fake-muon pairs, at least one leg of which is required to *fail* the muon ID requirement, passing looser baseline and vertex cuts for both positive and negative lifetimes.

These are representative of various background contributions and thus are excellent control regions to test the method of background estimation. We compare

the estimated background with actual observation. The result of this cross check is summarized in Table 1. The agreement between predicted and observed number of background events in the signal region is good across all of our control regions. The backgrounds were estimated using the same method as for the signal sample.

sample	NN cut	CMU-CMU			CMU-CMX		
		pred	obsv	prob(%)	pred	obsv	prob(%)
OS-	$0.80 < \nu_{NN} < 0.95$	$275 \pm (9)$	287	26	$310 \pm (10)$	304	39
	$0.95 < \nu_{NN} < 0.995$	$122 \pm (6)$	121	46	$124 \pm (6)$	148	3.2
	$0.995 < \nu_{NN} < 1.0$	$44 \pm (4)$	41	36	$31 \pm (3)$	50	0.4
SS+	$0.80 < \nu_{NN} < 0.95$	$2.7 \pm (0.9)$	1	29	$2.7 \pm (0.9)$	0	10
	$0.95 < \nu_{NN} < 0.995$	$1.2 \pm (0.6)$	0	34	$1.2 \pm (0.6)$	1	66
	$0.995 < \nu_{NN} < 1.0$	$0.6 \pm (0.4)$	0	55	$0.0 \pm (0.0)$	0	-
SS-	$0.80 < \nu_{NN} < 0.95$	$8.7 \pm (1.6)$	9	49	$5.7 \pm (1.6)$	2	11
	$0.95 < \nu_{NN} < 0.995$	$3.0 \pm (1.0)$	4	36	$3.6 \pm (1.0)$	2	34
	$0.995 < \nu_{NN} < 1.0$	$0.9 \pm (0.5)$	0	43	$0.3 \pm (0.3)$	0	70
FM+	$0.80 < \nu_{NN} < 0.95$	$169 \pm (7)$	169	50	$73 \pm (5)$	64	19
	$0.95 < \nu_{NN} < 0.995$	$55 \pm (4)$	43	9	$19 \pm (2)$	18	49
	$0.995 < \nu_{NN} < 1.0$	$20 \pm (2)$	20	48	$3.6 \pm (1.0)$	3	53

Table 1: The values given in the parentheses are the uncertainties on the mean of the background prediction. The Poisson probability for making an observation at least as large (or fewer than observed when observed is less than predicted) given the predicted background is also shown in the table. The best (blue) and worst (red) cases are also shown.

2.3.3 Results

The results from the CDF analysis on 3.7 fb^{-1} are shown in Table 2 and Figure 5. 6.1 ± 1.8 events were expected in the signal region and 7 events were observed, resulting in the observed limits, using 3 NN bins and 5 mass bins, shown in Table 2.

2.4 D0 Analysis with 6.1 fb^{-1} of Data

D0 uses a similar method as described above. For signal discrimination, variables are combined into a Bayesian Neural Network that also uses signal MC and data mass sidebands for optimization (Figure 6). Unlike CDF, D0 does not have the mass resolution to distinguish between B_d^0 and B_s^0 .

Channel	Expected	Observed
B_s^0 Central	4.0 ± 1.0	3
B_s^0 Extended	2.1 ± 0.8	4
B_d^0 Central	5.3 ± 1.0	5
B_d^0 Extended	2.8 ± 0.8	3

	90% CL	95% CL
B_s^0	3.6×10^{-8}	4.3×10^{-8}
B_d^0	6.0×10^{-9}	7.6×10^{-9}

Table 2: B_s^0 and B_d^0 expected and observed number of candidates in central and extended mass region (top) as well as resulting observed limits (bottom).

The D0 results are shown in Figure 7. 51 ± 4 background events are expected in the highest sensitivity region and 55 events are observed. The expected B_s^0 limit is 3.8×10^{-8} at 95% CL observed a limit of 5.1×10^{-8} .

2.5 CDF Improvements

CDF is working on an improved analysis with significantly more (3.2 fb^{-1}) data. The forward muon acceptance (left of Figure 8) has been increased and the neural network has been improved to achieve greater background rejection. The peaking background prediction has also been improved. The central-forward (CMU-CMX) channel of the analysis has increased in statistics by $\sim 15\%$ resulting in a total increase for both channels of $\sim 7\%$. The neural network has been improved by increasing the background rejections (Figure 9). Additionally the neural network has been extensively tested for mass bias (Figure 10).

The following variables, shown in order of significance to NN separation power, are used to discriminate the $B_s^0 \rightarrow \mu^+ \mu^-$ signal from the background:

$\Delta\alpha$: the 3D opening angle between the B_s^0 flight direction, $\vec{p}(B)$, and the direction of the decay vertex - estimated as the vector originating at the primary vertex and terminating at the muon-pair vertex;

Iso: the isolation of the candidate B_s^0 defined as, $Iso = p_T^{B_s^0} / (p_T^{B_s^0} + \sum_i p_T^i (\Delta R < 1.0))$, where the sum is over all tracks within an $\eta - \phi$ cone of radius $R = 1.0$, centered on $\vec{p}(B)$;

$|\mathbf{d}_0(\mu_1)|$: impact parameter of muon which has the larger value of the muon pair;

$|\mathbf{d}_0(\mathbf{B}_s^0)|$: impact parameter of B_s^0 reconstructed from muon pair;

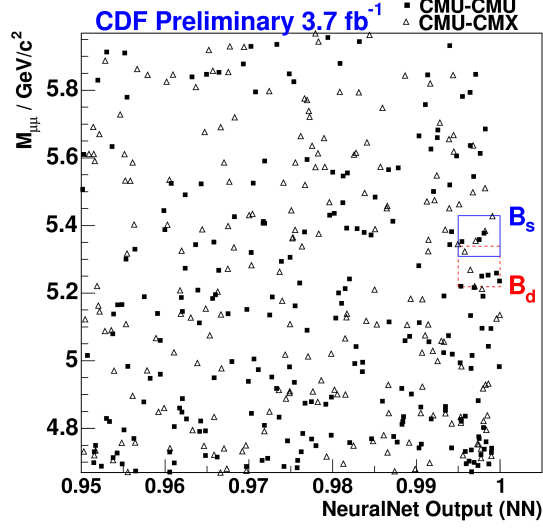


Figure 5: Di-muon mass vs NN output distribution for central-central (CMU-CMU) and central-forward (CMU-CMX) muons for CDF analysis.

$L_{2d}/\sigma_{L_{2d}}$: significance of L_{2d} ;

χ^2_{vtx} : χ^2 of the vertex;

L_{3D} : 3-dimensional vertexes displacement obtained by the vertex fitting;

$p_T(\mu_2)$: the transverse momentum of lower momentum daughter muon;

$|d_0(\mu_2)|/\sigma_{d_0(\mu_2)}$: Significance of smaller $|d_0(\mu)|$ of the muon with smaller impact parameter, where $\sigma_{d_0(\mu)}$ is estimated uncertainty of $|d_0(\mu)|$;

λ/σ_λ : proper decay length significance (λ divided by the uncertainty on λ);

λ : the proper decay length;

$|d_0(\mu_1)|/\sigma_{d_0(\mu_1)}$: significance of larger $|d_0(\mu)|$ of the muon with larger impact parameter, where $\sigma_{d_0(\mu)}$ is estimated uncertainty of $|d_0(\mu)|$;

$\Delta\alpha_{xy}$: the 2D opening angle between the B_s^0 flight direction, $\vec{p}(B)$, and the direction of the decay vertex - estimated as the vector originating at the primary vertex and terminating at the muon-pair vertex;

$|d_0(\mu_2)|$: impact parameter of muon which has the smaller value of the muon pair.

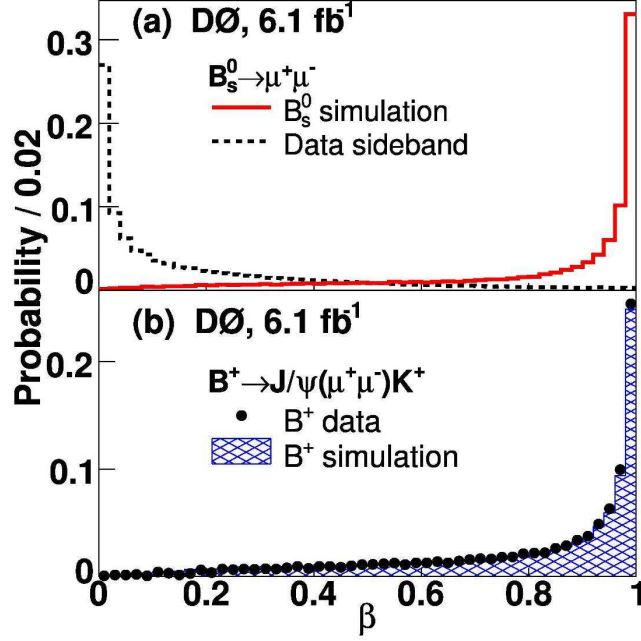


Figure 6: Distribution of Bayesian neural network output for signal MC and data mass sideband for D0 analysis.

The final NN network consists of 14 input variables. Extensive cross checks were done to demonstrate the 14-variable network does not sculpt the di-muon invariant mass distribution. Figure 10 shows the correlation across the $M_{\mu^+\mu^-}$ -mass range. No significant correlations are seen.

2.6 Expected Limits for CDF

A comparison of the previous expected and observed limits is shown in Table 3. The expected limit after including the new data set, the increased acceptance, and the NN improvements is about $\mathcal{B}(B_s^0 \rightarrow \mu^+\mu^-) \sim 2 \times 10^{-8}$.

	Expected	Observed
2fb^{-1}	4.9×10^{-8}	5.8×10^{-8}
3.7fb^{-1}	3.3×10^{-8}	4.3×10^{-8}
6.9fb^{-1}	$\sim 2 \times 10^{-8}$	-

Table 3: CDF expected and observed limits.

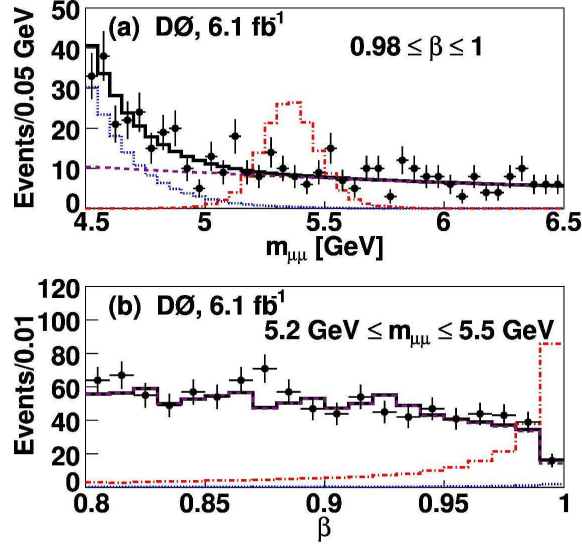


Figure 7: D0 unblinded di-muon mass distributions. The dots with error are the data, the solid black line is the expected number of background events, the red dotted-dashed lines is the SM signal $\times 100$, the dashed line is $B(D) \rightarrow \mu^+\nu X$ and $\overline{B}(\overline{D}) \rightarrow \mu^-\overline{\nu}X'$, and the blue dotted line is $B \rightarrow \mu^+\nu\overline{D}$ and $\overline{D} \rightarrow \mu^-\overline{\nu}X$

3 Conclusion

FCNC's are powerful probe for New Physics and CDF and D0 continue to lead the searches in the B sector. CDF is updating their $B_{s,d}^0 \rightarrow \mu^+\mu^-$ analysis which will significantly improve the expected limit for $\mathcal{B}(B_{s,d}^0 \rightarrow \mu^+\mu^-)$. CDF also has the first observation of $B_s^0 \rightarrow \mu^+\mu^-\phi$ as well as a A_{FB} measurement that competes and agrees with the B-factory results. Shortly after the FPCP conference CDF updated both the $b \rightarrow s\mu^+\mu^-$ and $B_{s,d}^0 \rightarrow \mu^+\mu^-$ analysis [15, 2, 16].

References

- [1] J. T. Wei, *et al.* (BELLE Collaboration), Phys. Rev. Lett. **103**, 171801 (2009).
- [2] T. Aaltonen *et al.* (CDF Collaboration), *et al.*, arXiv:1108.0695v1 [hep-ex]
- [3] K. G. Wilson, Phys. Rev. **179**, 1499 (1969).
- [4] B. Aubert, *et al.* (BABAR Collaboration), Phys. Rev. D **79**, 031102 (2009).
- [5] B. Aubert, *et al.* (BABAR Collaboration), Phys. Rev. Lett. **102**, 091803 (2009).

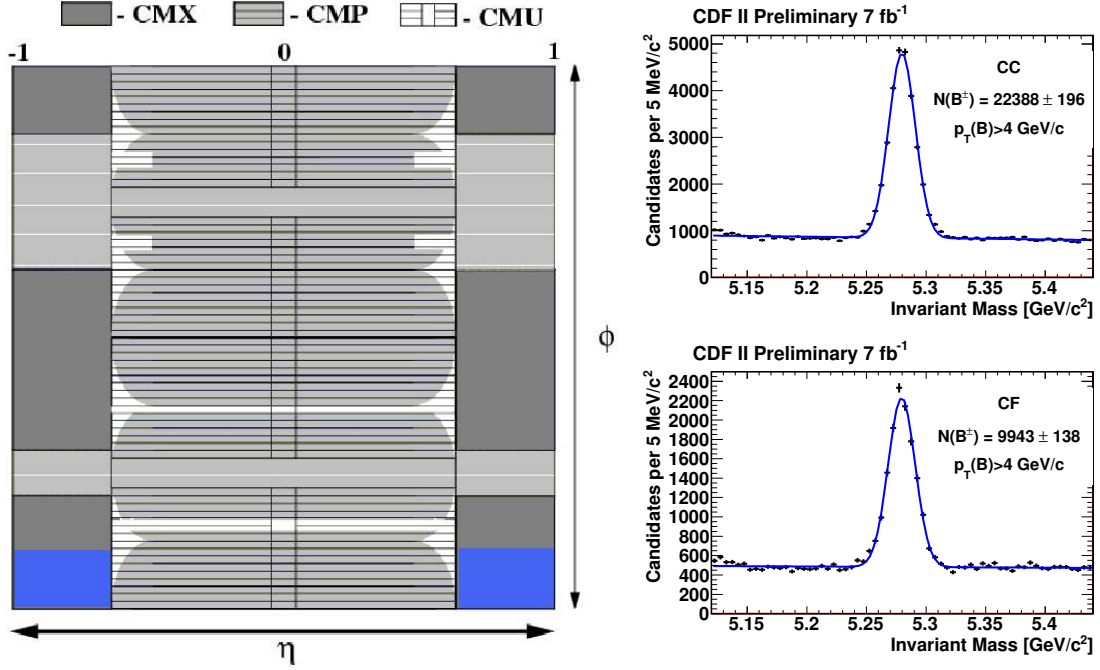


Figure 8: **Left:** CDF Muon detector layout. The blue region has been added for the updated analysis. **Right:** The $\mu^+\mu^-K^+$ invariant mass distribution for events satisfying the baseline and vertex requirements for the $B^+ \rightarrow J/\psi K^+$ sample.

- [6] A. Buras, B. Duling, T. Feldmann, T. Heidsieck, C. Promberger, S. Recksiegel, J. High Energy Phys. **1009**, 106 (2010) .
- [7] CDF Collaboration, *et al.*, A Search for $B_{s,d}^0 \rightarrow \mu^+\mu^-$ Decays Using 3.7 fb^{-1} of Data, CDFNOTE 9860.
- [8] V. M. Abazov, *et al.*, Phys. Lett. B **693**, 539 (2010)
- [9] S. R. Choudhury and N. Gaur, Phys. Lett. B **451**, 86 (1999); K. S. Babu and C. Kolda, Phys. Rev. Lett. **84**, 228 (2000).
- [10] R. Arnowitt *et al.*, Phys. Lett. B **538**, 121 (2002).
- [11] S. Baek *et al.*, J. High Energy Phys. **0506**, 017 (2005).
- [12] R. Ruiz de Austri *et al.*, J. High Energy Phys. **0605**, 002 (2006); J. Ellis *et al.*, J. High Energy Phys. **0605**, 063 (2006).
- [13] P. H. Chankowski and J. Rosiek, Acta Phys. Pol. B **33**, 2329 (2002).
- [14] K. Nakamura *et al.* (Particle Data Group), J. Phys. G **37**, 075021 (2010).

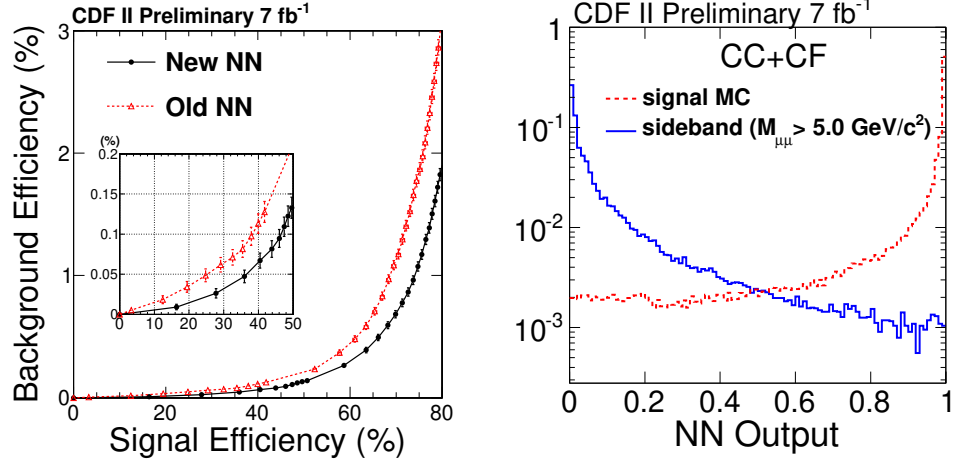


Figure 9: **Left:** Signal and background efficiency for both the old and new neural network. **Right:** The distribution of NN output for CC and CF combined. The red histogram is the signal MC, the black histogram is sideband data.

[15] T. Aaltonen *et al.* (CDF Collaboration), arXiv:1107.2304v1 [hep-ex]

[16] T. Aaltonen *et al.* (CDF Collaboration), arXiv:1107.3753v1 [hep-ex]

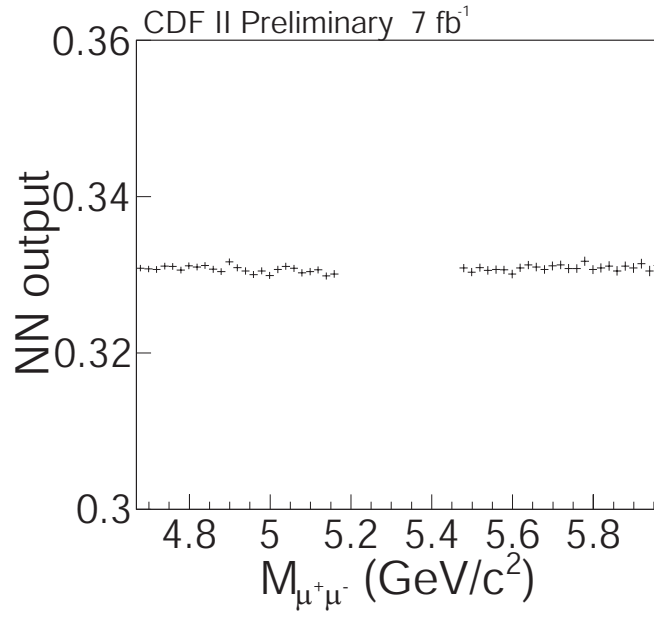


Figure 10: The top plot shows the NN output distributions for background (black histogram) and background trained as “signal” (red histogram). The bottom plot shows NN output as a function of di-muon invariant mass.